A&A 540, A122 (2012)
DOI: 10.1051/0004-6361/201016349

Astronomy & Astrophysics

Expected constraints on the Galactic magnetic field using *Planck* data

L. Fauvet[1,2], J. F. Macías-Pérez[2], T. R. Jaffe[5], A. J. Banday[5], F. X. Désert[2,3,4], and D. Santos[2]

[1] European Space Agency (ESA), Research and Scientific Support Dpt., Astrophysics Division, Keplerlaan 1, 2201AZ Noordwijk, The Netherlands
e-mail: lfauvet@rssd.esa.int
[2] LPSC, Université Joseph Fourier Grenoble 1, CNRS/IN2P3, Institut National Polytechnique de Grenoble, 53 avenue des Martyrs, 38026 Grenoble Cedex, France
[3] IPAG, Institut de Planétologie et d'Astrophysique de Grenoble, UJF-Grenoble 1 CNRS/INSU, UMR 524, 38041 Grenoble, France
[4] Institut Néel, 25 rue des Martyrs, BP 166, 38042 Grenoble Cedex 9, France
[5] Institut de Recherche en Astrophysique et Planétologie, Université de Toulouse (UPS-OMP), CNRS, UMR 5277, 9 Av. du colonel Roche, 31028 Toulouse, France

Received 17 December 2010 / Accepted 27 January 2012

ABSTRACT

Aims. We explore the ability to constrain the Galactic magnetic field intensity and spatial distribution with the incoming data from the *Planck* satellite.
Methods. We performed realistic simulations of the *Planck* observations at the polarised frequency bands from 30 to 353 GHz for two all-sky surveys in the same way that we expected to turn out for the nominal mission. These simulations include cosmic microwave background (CMB), synchrotron and thermal dust Galactic emissions and instrumental noise. (Note that systematic effects are not considered in this paper.) For the synchrotron and thermal dust Galactic emissions we used a coherent 3D model of the Galaxy that describes its matter density and the magnetic field direction and intensity. We first simulated the synchrotron and dust emissions at 408 MHz and 545 GHz, respectively, and then extrapolated them to the *Planck* frequency bands.
Results. We performed a likelihood analysis to compare the simulated data to a set of models obtained by varying the pitch angle of the regular magnetic field spatial distribution, the relative amplitude of the turbulent magnetic field, the radial scale of the electron and dust grain distributions, and the extrapolation spectral indices for the synchrotron and thermal dust emissions. We are able to set tight constraints on all considered parameters. We also found that the observed spatial variations of the synchrotron and thermal dust spectral indices will probably not affect our ability to recover the other parameters of the model.
Conclusions. From this, we conclude that the *Planck* satellite experiment can precisely measure the main properties of the Galactic magnetic field. For an accurate reconstruction of the matter distribution one still requires on the one hand an improved modelling of the interstellar medium and on the other hand such as extra data sets rotation measurements of pulsars.

Key words. cosmology: observations – ISM: clouds – methods: data analysis – magnetic fields – submillimeter: ISM – ISM: general

1. Introduction

The *Planck* satellite (Planck Collaboration 2011a; Tauber et al. 2010), currently in flight, will provide measurements of the CMB anisotropies in temperature and polarisation over the full sky at unprecedented accuracy Planck Collaboration (2011a); Tauber et al. (2010). It covers a wide range of frequencies from 30 to 857 GHz and therefore is able to give a measurement of the foreground emissions. *Planck* observes the sky with a combined sensitivity of $\Delta T/T_{\rm CMB} \sim 2 \times 10^{-6}$ (Planck Collaboration 2005) and an angular resolution from 33 to 5 arcmin (Planck Collaboration 2005). In particular, because of its seven polarised channels it will for the first time allow the simultaneous precise measurement of the main sources of polarised Galactic emissions: synchrotron and thermal dust.

Using the WMAP (*Wilkinson* Microwave Anisotropy Probe), Page et al. (2007) have shown that the synchrotron emission is highly polarised, up to 70% between 23 and 94 GHz. Furthermore, Benoît et al. (2004) and Ponthieu et al. (2005) have observed significantly polarised thermal dust emission, up to 15% in the 353 GHz Archeops channel. The free-free emission is not intrinsically polarised and the anomalous dust-correlated emission is weakly polarised at $3^{+1.3}_{-1.9}$ (Battistelli et al. 2006). At the *Planck* frequency bands the polarised contribution from compact and point sources is expected to be weak for both radio (Nolta 2009) and dusty (Désert et al. 1990) sources. The frequency and spatial distributions of the polarised diffuse Galactic emissions are not well known at present and the only available information comes from microwave and submillimeter observations.

The Galactic synchrotron emission originates from relativistic electrons that spirale along magnetic field lines. The direction of polarisation is orthogonal to the line-of-sight as well as to the field lines.

The synchrotron emission principally contributes to diffuse emission at radio and microwave observation frequencies. Its spectral energy distribution (SED) is not known with accuracy but it is assumed to be satisfactorily reproduced by a power law in antenna temperature $T_\nu \alpha \nu^{\beta_s}$ with a spectral index ranging form –2.7 to –3.4 (Lawson et al. 1987; Reich & Reich 1988; Reich et al. 2004; Kogut et al. 2007; Gold et al. 2009; Fauvet et al. 2010). The Galactic synchrotron emission has been successfully traced by the Leiden survey between 408 MHz and

1.4 GHz (Brouw & Spoelstra 1976; Wolleben et al. 2006), the Parkes survey at 2.4 GHz (Duncan et al. 1999), and the MGLS (Medium Galactic Latitude Survey) at 1.4 GHz (Uyaniker et al. 1999). At the microwave frequencies it has been mapped by WMAP, see e.g. Hinshaw et al. (2009) and Page et al. (2007).

Thermal dust emission arises from dust grains in the interstellar medium (ISM) with typical sizes $\simeq 0.25$ μm that are heated by stellar radiation (Désert et al. 1990). This emission can be partially polarised because prolate dust grains align with their long axis perpendicular to the magnetic field (Davis & Greenstein 1951). The dust emission efficiency is greatest along the long axis, leading to partial linear polarisation perpendicular to the magnetic field. The fractional polarisation depends on the grain size distribution and is typically a few percent at millimeter wavelengths (Hildebrand et al. 1999; Vaillancourt 2002; Fauvet et al. 2010). The thermal dust emission in intensity has already been accurately measured by IRAS form 5 to 100 μm (Neugebauer et al. 1984) and COBE/FIRAS which provided the first polarised observation at high frequencies. Currently, *Planck* High Frequency Instrument (HFI) (Planck HFI Core Team 2011) is measuring this emission in intensity (Planck Collaboration 2011b,c,d,e).

Based on the physical characteristics of the synchrotron emission, Page et al. (2007) proposed a 3D model of the Galaxy that includes the distribution of relativistic electron and the spatial distribution of the Galactic magnetic field. Independently, Han et al. (2004, 2006) used a 3D model of the free electrons density in the Galaxy (Cordes & Lazio 2002) and a model of the Galactic magnetic field including regular and turbulent components to explain the observed rotation measurements towards known pulsars. Based on these works Sun et al. (2008) performed a combined analysis of the rotation measurement of pulsars and of the polarised WMAP data. These authors' work has been extended by Jaffe et al. (2010) to study the Galactic plane and Jansson et al. (2009) for the full sky. Recently, Fauvet et al. (2010) proposed for the first time a coherent model of the synchrotron and thermal dust Galactic emissions using the WMAP and ARCHEOPS data. In addition to the above, many other related models and analyses can be found in the literature.

In this paper we propose a method to study and constrain the synchrotron and thermal dust polarised emissions using the *Planck* satellite observations that are currently made. Using realistic simulations of the *Planck* polarised data, we forecast the expected constraints on a 3D model of the Galactic magnetic field and the Galactic matter distribution. This paper is structured as follows: in Sect. 2.1 we describe the models we used for the polarised components of the Galactic diffuse emissions, and in Sect. 3 we present the simulations of data used in this analysis. In Sect. 4 we describe our method to constrain these Galactic foreground emission models and we discuss the results in Sect. 5. Conclusions are presented in Sect. 6.

2. Models of polarised Galactic emissions

A realistic model of synchrotron and thermal dust emissions can be constructed from a 3D description of the Galaxy including the matter distribution and the magnetic field structure. Following Fauvet et al. (2010), we calculated the Stokes parameters I, Q and U of the emerging polarised Galactic emissions along the line-of-sight $\boldsymbol{n}$.

We used the following model (Fauvet et al. 2010) for the synchrotron emission, in galactocentric cylindrical coordinates (r, ϕ, z):

$$
\begin{aligned}
I_{\rm sync}(\boldsymbol{n}) &= I_{\rm Has/ff}(\boldsymbol{n})\left(\frac{\nu_s}{0.408}\right)^{\beta_s},\\
Q_{\rm sync}(\boldsymbol{n}) &= I_{\rm Has/ff}(\boldsymbol{n})\left(\frac{\nu_s}{0.408}\right)^{\beta_s}\\
&\quad\times\frac{\int\cos(2\gamma(\boldsymbol{n},s))p_s\left(B_l^2(\boldsymbol{n},s)+B_t^2(\boldsymbol{n},s)\right)n_{\rm CRE}(r,z){\rm d}s}{\int\left(B_l^2(\boldsymbol{n},z)+B_t^2(\boldsymbol{n},s)\right)n_{\rm CRE}(r,z){\rm d}s},\\
U_{\rm sync}(\boldsymbol{n}) &= I_{\rm Has/ff}(\boldsymbol{n})\left(\frac{\nu_s}{0.408}\right)^{\beta_s}\\
&\quad\times\frac{\int\sin(2\gamma(\boldsymbol{n},s))p_s\left(B_l^2(\boldsymbol{n},s)+B_t^2(\boldsymbol{n},s)\right)n_{\rm CRE}(r,z){\rm d}s}{\int\left(B_l^2(\boldsymbol{n},s)+B_t^2(\boldsymbol{n},s)\right)n_{\rm CRE}(r,z){\rm d}s},
\end{aligned}
$$

where $B_n(\boldsymbol{n}, s)$ is the magnetic component along the line-of-sight $\boldsymbol{n}$, and $B_l(\boldsymbol{n}, s)$ and $B_t(\boldsymbol{n}, s)$ the magnetic field components on a plane perpendicular to the line-of-sight. The polarisation fraction p_s is set to 75% (Rybicki & Lightman 1979). The polarisation angle $\gamma(\boldsymbol{n}, s)$ is given by

$$
\gamma(\boldsymbol{n},s)=\frac{1}{2}\arctan\left(\frac{2B_l(\boldsymbol{n},s)\cdot B_t(\boldsymbol{n},s)}{B_l^2(\boldsymbol{n},s)-B_t^2(\boldsymbol{n},s)}\right), \tag{1}
$$

the distribution of relativistic electrons, $n_{\rm CRE}$, is described in detail in Sect. 2.1.1. $I_{\rm Has/ff}$ is a template temperature map obtained from the 408 MHz all-sky continuum survey (Haslam et al. 1982). This map also includes bremsstrahlung (free-free) emission. To substract this component, we used the WMAP K-band free-free foreground map generated from the maximum entropy method (MEM) (Hinshaw et al. 2007; Bennett et al. 2003). Note that this template is not necessarily realistic; Alves et al. (2010) have shown with radio recombination lines that in at least one region in the Galactic plane, this model appears to overestimate the amount of free-free emission. However, this will not have any impact in the following analysis because we used the same template in the simulated data and in the fitted models and the uncertainty at 408 MHz is very small compared to the synchrotron amplitude. The free-free map was then extrapolated to 408 MHz assuming a power law dependence as in Dickinson et al. (2003). The spectral index β_s used to extrapolate maps at various frequencies is a free parameter of the model and will be discussed later.

For the thermal dust emission we used the following model (Fauvet et al. 2010):

$$
\begin{aligned}
I_{\rm dust}(\boldsymbol{n}) &= I_{\rm fds}(\boldsymbol{n})\left(\frac{\nu_{\rm d}}{353}\right)^{\beta_{\rm d}},\\
Q_{\rm dust}(\boldsymbol{n}) &= I_{\rm fds}(\boldsymbol{n})\left(\frac{\nu_{\rm d}}{353}\right)^{\beta_{\rm d}}\\
&\quad\times\frac{\int\cos(2\gamma(\boldsymbol{n},s))\sin^2(\alpha)f_{\rm norm}p_{\rm d}n_{\rm dust}(r,z){\rm d}s}{\int n_{\rm dust}(r,z){\rm d}s},\\
U_{\rm dust}(\boldsymbol{n}) &= I_{\rm fds}(\boldsymbol{n})\left(\frac{\nu_{\rm d}}{353}\right)^{\beta_{\rm d}}\\
&\quad\times\frac{\int\sin(2\gamma(\boldsymbol{n},s))\sin^2(\alpha)f_{\rm norm}p_{\rm d}n_{\rm dust}(r,z){\rm d}s}{\int n_{\rm dust}(r,z){\rm d}s},
\end{aligned}
$$

where the dust polarisation fraction $p_{\rm d}$ is set to 10% (Ponthieu et al. 2005), and $n_{\rm dust}(r, z)$ is the dust grain distribution discussed in Sect. 2.1.1. The $\sin^2(\alpha)$ term accounts for geometrical

supression and $f_{\rm norm}$ is an empirical factor that accounts for the misalignment between dust grains and the magnetic field lines (see Fauvet et al. 2010, for details). The reference map, $I_{\rm fds}$, is the Finkbeiner et al. (1999) model 8 prediction based on IRAS (Neugebauer et al. 1984) and on COBE/DIRBE data. The spectral index $\beta_{\rm d}$ used to extrapolate maps at various frequencies is a free parameter of the model. This template seems to be a good representation of the ARCHEOPS data at 353 GHz as discussed in Macías-Pérez et al. (2007). Notice that for the polarised *Planck* frequencies, we are in the Rayleigh-Jeans domain and can therefore use, a power-law approximation for the dust intensity.

2.1. 3D model of the Galaxy

We here describe our 3D model of the Galaxy.

2.1.1. Matter density

We consider an exponential distribution of relativistic electrons $n_{\rm CRE}$ on the Galactic disc as described by Drimmel & Spergel (2001):

$$n_{\rm CRE}(r,z) = n_{0,\rm e}\frac{\mathrm{e}^{-\frac{r}{n_{\rm CRE,r}}}}{\cosh^2(z/n_{\rm CRE,h})}, \quad (2)$$

where $n_{\rm CRE,r}$ is the scale radius of the distribution and is a free parameter of the model. The vertical scale height, $n_{\rm CRE,h}$, is set to 1 kpc. The value of $n_{0,\rm e}$ is set to 6.4×10^{-6} cm^{-3}, following Sun et al. (2008).

The distribution of dust grains $n_{\rm dust}$ is described in the same way as that of relativistic electrons with

$$n_{\rm dust}(r,z) = n_{0,\rm d}\frac{\mathrm{e}^{-\frac{r}{n_{\rm d,r}}}}{\cosh^2(z/n_{\rm d,h})}, \quad (3)$$

where the scale radius $n_{\rm d,r}(r,z)$ is also a free parameter of the model (see Fauvet et al. 2010, for more details). The vertical scale height, $n_{\rm d,r}$, is set to 1 kpc.

2.1.2. Galactic magnetic field model

The Galactic magnetic field model is composed of two parts: a regular component and a turbulent component, such that $\boldsymbol{B} = \boldsymbol{B}_{\rm reg} + \boldsymbol{B}_{\rm turb}$ (bold letters indicate vectorial quantities). We included only the isotropic part of the turbulent magnetic field and no anisotropic/ordered component (see Jaffe et al. 2010). As in Fauvet et al. (2010), our regular component is then equivalent to the sum of what Jaffe et al. (2010) call the coherent and ordered fields. For this analysis of synchrotron and dust emission only, the distinction is irrelevant. For the regular component we considered a modified logarithmic spiral model (MLS), presented in Fauvet et al. (2010) and based on the WMAP model (Page et al. 2007). In cylindrical coordinates (r,ϕ,z) it reads

$$\begin{aligned}\boldsymbol{B}_{\rm reg}(r) \;=\; & B(r)[\cos(\phi+\beta)\ln\left(\frac{r}{r_0}\right)\sin(p)\cos(\chi(r))\cdot\boldsymbol{u}_r \\ & -\cos(\phi+\beta)\ln\left(\frac{r}{r_0}\right)\cos(p)\cos(\chi(r))\cdot\boldsymbol{u}_\phi \\ & +\sin(\chi(r))\cdot\boldsymbol{u}_z], \end{aligned} \quad (4)$$

where the pitch angle, p, is a free parameter of the model and $\beta = 1/\tan(p)$. The scale radius r_0 is set to 7.1 kpc and $\chi(r) = \chi_0(r)(z/z_0)$ is the vertical scale height, with $\chi_0 = 22.4$ degrees and $z_0 = 1$ kpc. The intensity of the regular field is fixed with the pulsar Faraday rotation measurements by Han et al. (2006):

$$B(r) = B_0\,\mathrm{e}^{-\frac{r-R_\odot}{R_B}}, \quad (5)$$

where the large-scale field intensity at the Sun position is $B_0 = 2.1\pm0.3$ μG and $R_B = 8.5\pm4.7$ kpc. The distance between the Sun and the Galactic centre, $R_\odot$ is set to 8 kpc following Eisenhauer et al. (2003) and Reid & Brunthaler (2005).

2.1.3. Turbulent component

In addition to the large-scale Galactic magnetic field, Faraday rotation measurements on pulsars in our vicinity have revealed a turbulent component (Lyne & Smith 1989; Han et al. 2004) with an amplitude estimated to be of the same order of magnitude as that of the regular one (Han et al. 2006).

The turbulent magnetic field is assumed to be a 3D anisotropic Gaussian random vectorial field and it is fully determined by a spherically symmetric power spectrum in the Fourier domain. Indeed, the magnetic energy $E_B(k)$ associated with the turbulent component can be described by a power spectrum of the form (Han et al. 2004, 2006)

$$E_B(k) = C\left(\frac{k}{k_0}\right)^\alpha, \quad (6)$$

where $\alpha = -0.37$ and $C = (6.8\pm0.3)\times10^{-13}$ erg cm^{-3} kpc. More complex models of this anisotropic turbulent component have been proposed by Higdon (1984); Cho et al. (2002) and Cho & Lazarian (2010), but they are beyond the scope of this paper. Note also that we did not consider here the so-called ordered turbulent component of the Galactic magnetic field the way it is discussed in Jaffe et al. (2010).

3. Simulated data

We have performed simulations of the *Planck* polarised observations. We considered the entire polarised channels for the Low Frequency Instrument (LFI) (Bersanelli et al. 2010; Mandolesi et al. 2010; Menella et al. 2011) and HFI (Lamarre et al. 2010; Planck HFI Core Team 2011) instruments at 30, 44, 70, 100, 143, 217, and 353 GHz for two full-sky surveys (14 months). We did not use the total intensity maps in this analysis. For this set of simulations we generated full-sky maps in the HEALPix pixelisation scheme (Górski et al. 2005) at $N_{\rm side} = 128$. The input templates were simply degraded to that resolution using the HEALPix tools.

At a given observation frequency, ν, we consider that the polarised observations (X^ν) are the sum of the synchrotron ($X^\nu_{\rm sync}$) and the thermal dust emissions ($X^\nu_{\rm dust}$), where X is the Q or U Stokes parameter. We also add a CMB contribution ($X^\nu_{\rm CMB}$) and noise ($X^\nu_{\rm N}$) so that can finally write $X^\nu = X^\nu_{\rm dust} + X^\nu_{\rm sync} + X^\nu_{\rm N} + X^\nu_{\rm CMB}$.

3.1. Polarised Galactic emission components

The polarised Galactic emissions were simulated using the 3D model described in Sect. 2.1. The parameters of the 3D model of the Galaxy were taken from Fauvet et al. (2010) by comparison with the available ARCHEOPS (Benoît et al. 2004) and WMAP five-year data (Hinshaw et al. 2009). The pitch angle

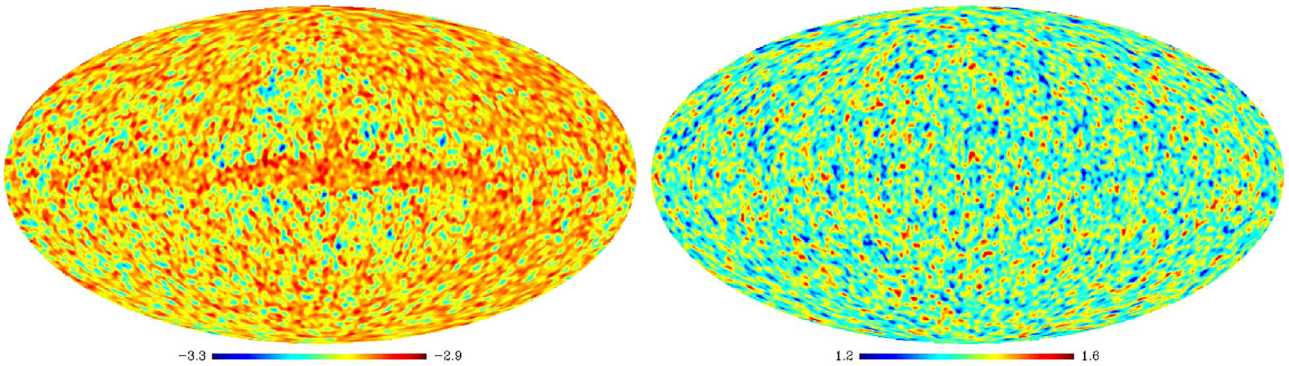

Fig. 1. Spatial variations of the spectral indices for the simulated synchrotron (*left*) and thermal dust Galactic polarised emissions (*right*).

Table 1. Summary of the different types of simulations.

Simulation	$\beta_{s,d}$	$A_{\rm turb}$
Simu 1	constant	$0.0 \times B_{\rm reg}$
	variable	$0.0 \times B_{\rm reg}$
Simu 2	constant	$0.25 \times B_{\rm reg}$
	variable	$0.25 \times B_{\rm reg}$

was set to –30 degrees and the radial widths of the distributions of dust grains $n_{\rm d,r}$ and ultrarelativist electrons $n_{\rm CRE,r}$ were set to 3 kpc. We computed simulated data with a model of Galactic magnetic field with (*Simu I*) or without a turbulent component (*Simu II*). In the first case we set the amplitude of the turbulent component to $A_{\rm turb} = 0.25 \times B(r)$. The simulations were extrapolated to each of the *Planck* frequencies assuming constant spectral indices in frequency and using two different configurations, either spatially constant (*Simu Cst*) or variable (*Simu Var*), accross the sky. We produced at least ten simulations for each of the different configurations.

In the *Simu Cst* case we set the value of the synchrotron spectral index to $\beta_s = -3.0$. We tested teh upper and lower expected limits of the spectral index for the thermal dust emission. Concerning the thermal dust emission we test both upper and lower expected limits of the spectral index. We tested 1.4 as a lower limit, obtained by comparison of a grey body law model to the Archeops and Iris data in the galactic plane. The upper limit tested is 2, following results obtained at high latitude by Boulanger et al. (1996) using the Firas and Dirbe data.

For the *Simu Var* case, the maps of β_s and $\beta_{\rm d}$ were built in the following way. For the synchrotron emission we used the map generated using a MCMC fit by Kogut et al. (2007) at 23 GHz, but applyied some corrections. We cut all pixels where $\beta_s < -3.5$ and $\beta_s > -2.8$, following the results in Page et al. (2007); Sun et al. (2008) and Fauvet et al. (2010), and assumed for those pixels $\beta_s = -3.0 + 0.1 * n$, where n is a Gaussian random normal distribution. Note that β_s is the typical average value found in the literature. It is also important to clarify that this spectral index map was not derived from the MEM analysis of the WMAP data. However, it can be used as a fair representation of the variability of the spectral index. The resulting synchrotron spectral index map is shown in the left panel of Fig. 1.

To simulate the spatial variations of the spectral index of the thermal dust emission, we assumed a random Gaussian distribution with a mean value of $\beta_{\rm d,mean} = 1.4$ or $\beta_{\rm d,mean} = 2.0$ and a standard deviation of 0.3. The right panel of Fig. 1 shows the resulting thermal dust spectral index map. Table 1 summarises the resulting types of simulations that we carried out.

3.2. CMB emission

We produced maps at $N_{\rm side} = 128$ of the expected CMB signal at all *Planck* frequencies. We used CAMB (Lewis et al. 2000) to compute the CMB temperature and polarisation angular power spectra for the WMAP ΛCDM best-fit model as estimated by Komatsu et al. (2009). We also took into account gravitational lensing effects and assumed a tensor-scalar ratio, r, of 0.1 (Efstathiou et al. 2009).

3.3. Noise

Planck noise maps for each of the frequency channels were computed using the mean sensitivity per pixel given in Table 2. We assumed isotropic random Gaussian noise accross the sky. This is different from the case for the real *Planck* scanning strategy (Dupac 2005). However it should not have any impact on the presented results because our data are mostly signal-dominated.

4. Method

Following Fauvet et al. (2010), we computed Galactic profiles in polarisation to compare the models of Galactic polarised emissions to the *Planck* data simulations we computed Galactic profiles in polarisation using the set of latitude bands (in degrees) [0, 30], [30, 60], [60, 90], [90, 120], [120, 180], [180, 270], [270, 330], [330, 360]. Note that we did not used the intensity profiles because the intensity maps were constructed with fixed templates.

Galactic latitude profiles for the diffuse Galactic polarised emission models were computed for a grid of models obtained by varying the pitch angle, p, the turbulent component amplitude, $A_{\rm turb}$, the radial scale for the distribution of electrons, $n_{\rm CRE,r}$ and of dust grains $n_{\rm d,r}$, and the spectral indices β_s and $\beta_{\rm d}$. The latter were assumed to be spatially constant accross the sky. All other parameters were set to the values proposed in Sect. 3.1.

We compared the simulated data sets to the Galactic emission models using a likelihood analysis where the log-likelihood function is given by:

$$-\log \mathcal{L} = \frac{\sum_{\nu=0}^{nfreq-1} \sum_{i=0}^{nlon-1} \sum_{n=0}^{nlat-1} (S^{\nu}_{i,X}(n) - M^{\nu}_{i,X}(n))^2}{\sigma^{\nu}_{i,X}(n)^2 + \sigma^{\nu,\rm turb}_{i,X}(n)^2},$$

where the X are the Stokes parameters Q and U, and i and n index the longitude bands and the latitude bins, respectively. $S^{\nu}_{i,X}(n)$ and $M^{\nu}_{i,X}(n)$ are the set of simulations and models for the polarisation state X, i longitude band and n longitude bin respectively. The term $\sigma^{\nu}_{i,X}(n)^2$ is the error associated to $S^{\nu}_{i,X}(n)$ computed from the standard deviation of the data samples in each of

Table 2. Average 1σ sensitivity per pixel (a square whose side is the full width at half maximum (FWHM) extent of the beam) in thermodynamic temperature units, achievable after two full sky surveys (14 months) by *Planck*.

Centre frequency [GHz]	30	44	70	100	143	217	353
$(\Delta T/T)$ polarisation [μK/K]	2.8	3.9	6.7	4.0	4.2	9.8	29.8
Angular resolution [arcmin *FWHM*]	33	24	14	10	7	5	5

References. Planck Collaboration (2005).

Table 3. Parameters of the 3D Galactic polarised diffuse emission models.

Parameters	Range	Binning
p (deg)	$[-80.0, 80.0]$	10.0
$A_{\rm turb}$	$[0, 2.5] * B_{\rm reg}$	0.125
$n_{\rm CRE,r}$ (kpc)	$[1.0, 20.0]$	1
$n_{\rm d,r}$ (kpc)	$[1.0, 20.0]$	1
β_s	$[-4.3, -2.4]$	0.1
$\beta_{\rm d}$	$[2.0, 4.0]$	0.1

the latitude bins. Note that it accounts for the noise as well as for signal dispersion within the bin. The term $\sigma^{\nu,\rm turb}_{i,X}(n)$ accounts for the additional variance caused by the turbulent component of the magnetic field. Indeed, because the magnetic field is considered to be a random distribution, we need to take into account in the likelihood function as an extra correlation matrix. We approximated this matrix to a diagonal one. We used ten simulations of the Galactic turbulent contribution at each *Planck* frequency band to estimate $\sigma^{\nu,\rm turb}_{i,X}(n)$. Note that the latter term is proportional to $A_{\rm turb}$ and also to the extrapolation term, $(\frac{\nu}{\nu_{\rm ref}})^{\beta}$, for the synchrotron and thermal dust components. This may introduce a small bias in the $A_{\rm turb}$, β_s and $\beta_{\rm d}$ parameters. Increased turbulence can be balanced by a steeper spectral index and therefore it is possible to lower the resulting χ^2 for some parameter combinations. We will see, however, that the impact of this bias on the results remains small.

5. Results and discussion

The expected constraints on the parameters of the polarised Galactic emission models using the simulated *Planck* data are given in Tables 4 and 5 for the various sets of simulations.

5.1. Simu I

The constraints obtained for the *Simu I* cases are presented in the first line of Tables 4 and 5. The associated marginalised likelihood in 1 and 2D are shown in Fig. 2 for the parameters $A_{\rm turb}$, p, $n_{\rm CRE,r}$, $n_{\rm d,r}$, β_s and $\beta_{\rm d}$, and we present the 1, 2 and 3σ confidence level contours. Evidently, there is no correlation between the parameters. We are able to tightly constrain all the parameters of the Galactic emission models. Furthermore, we can see that the best fit values coincide with the parameters used in the input simulations. Therefore, there is no indication of bias in the method. We can see that spatial variations of the spectral indices do not disturb the constraints on the parameters. Indeed, the expected constraints on all parameters of the models, including the values of spectral indices, are unchanged. This could be because we used a Galactic-profile-based comparison, which is not very sensitive to pixel-to-pixel variations but rather to general features. The constraint on the dust grain density parameter is weaker than that for the relativistic electrons density. This is probably because the synchrotron emission is dominant at the *Planck* frequencies.

5.2. Simu II

The results for the *Simu II* cases, i.e. those including a turbulent component, are summarised in lines 3 and 4 of Tables 4 and 5. The marginalised likelihoods in 1 and 2D for the parameters $A_{\rm turb}$, p, $n_{\rm CRE,r}$, $n_{\rm d,r}$, β_s and $\beta_{\rm d}$ are shown in Fig. 3 where we present the 1, 2 and 3σ confidence level contours. We observe that there is no correlation between parameters, but, the constraints on the different parameters are weaker by a factor of 2 or more compared to the *Simu I* case. We observe a small bias on the best-fit values of the two spectral indices, but it is within the 1σ error bars; it is related to the additional noise-like term added to the likelihood calculation by the turbulent component of the magnetic field. Furthermore, the radial scales $n_{\rm CRE,r}$ and $n_{\rm d,r}$ are not constrained. A degeneracy between the matter distribution and the other parameters of the models is induced by the method of construction but is not visible in Fig. 3. Nevertheless, an upper limit can be set. Because the millimeter and submillimeter data are not very sensitive to changes in those parameters, as was discussed in Fauvet et al. (2010), only an upper limit can be determined.

6. Summary and conclusions

We proposed a method to estimate the expected constraints on the Galactic diffuse polarised emissions and the Galactic magnetic field at large scales using the *Planck* data. With this aim, we computed realistic simulations of the *Planck* data at the polarised frequency bands for two all-sky surveys. These simulations include CMB, synchrotron and thermal dust emissions, and instrumental noise. For the synchrotron and thermal dust Galactic emissions we used a coherent 3D model of the Galaxy that describes the magnetic field direction and intensity as well as the distribution of matter. The relativistic electron and dust grain densities were modelled using exponential distributions in galactocentric coordinates. For the Galactic magnetic field we considered the modified logarithmic spiral model discussed in Fauvet et al. (2010).

We performed a likelihood analysis to compare the simulated *Planck* data to a set of models obtained by varying the pitch angle of the regular magnetic field spatial distribution, the relative amplitude of the turbulent magnetic field, the radial scale of the electron and dust grain distributions as well as the extrapolation indices of the synchrotron and thermal dust emissions. We are able to set accurate constraints on most of the considered parameters. We also found that the observed spatial variations of the synchrotron and thermal dust spectral indices should not affect our ability to recover the other parameters of the model. The presence of a turbulent component of the Galactic magnetic

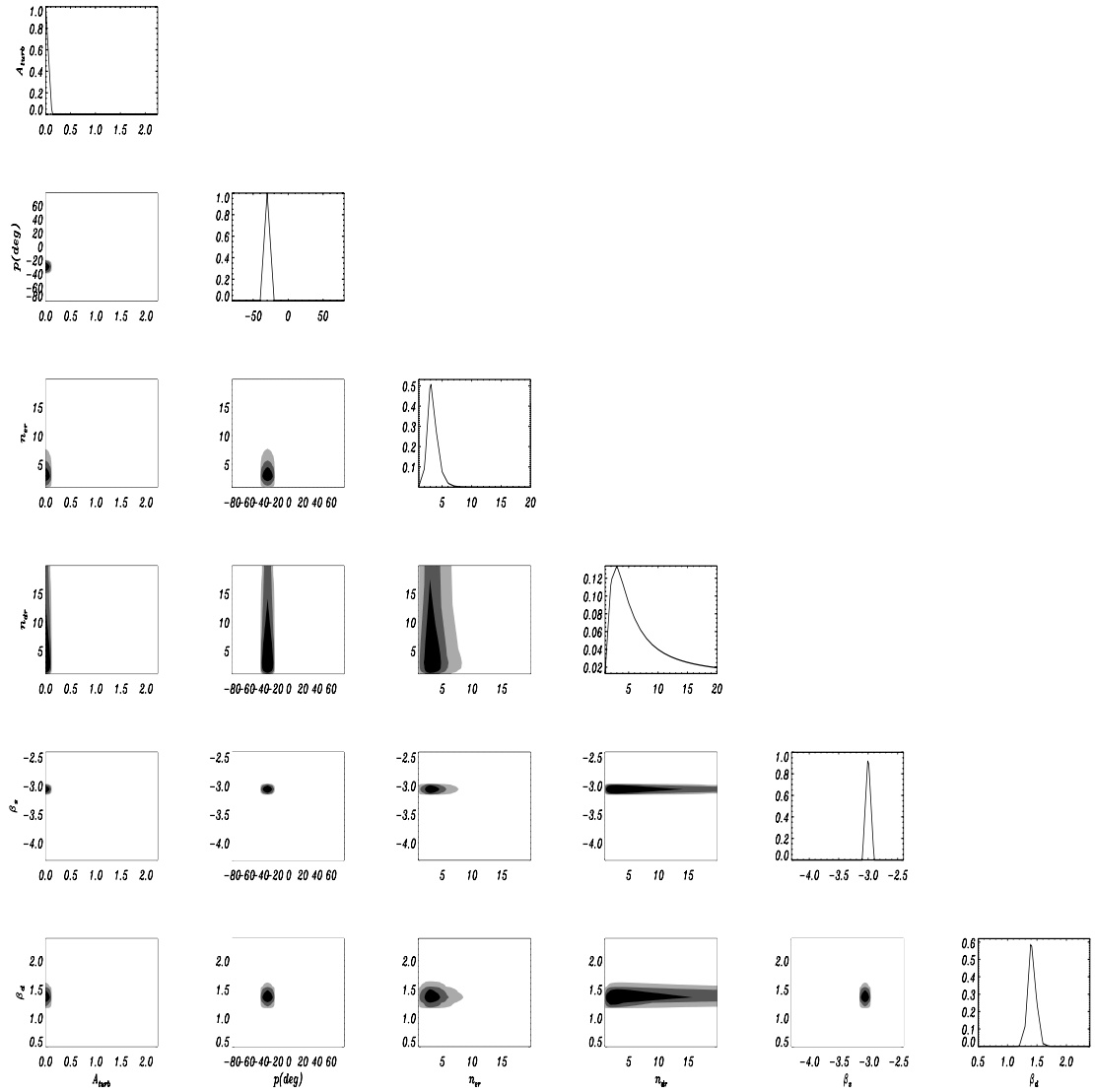

Fig. 2. Marginalised likelihood in 1 and 2D for the parameters $A_{\rm turb}$ and p, $n_{\rm CRE,r}$, $n_{\rm d,r}$, β_s and $\beta_{\rm d}$ for the (*Simu I Cst*) case present the 1 (68.8%), 2 (95.4%) and 3σ (98%) confidence level contours. The values of the parameters included in the simulated data are set to $A_{\rm turb} = 0$, $p = -30°$, $n_{\rm CRE,r} = n_{\rm d,r} = 3$ kpc, $\beta_s = -3.0$, $\beta_{\rm d} = 1.4$, respectively.

Table 4. Best-fit parameters for the Galactic polarised emission models for $\beta_{\rm d} = 1.4$ in the simulated data.

Simulation	Simu I		Simu II	
$\beta_{\rm simu}$	Cst	Var	Cst	Var
$A_{\rm turb}$	<0.1	<0.1	$0.25^{+0.2}_{-0.1}$	$0.25^{+0.2}_{-0.1}$
p(deg)	-30^{+4}_{-6}	-30^{+4}_{-6}	-30^{+8}_{-14} (5)	-30^{+8}_{-14} (5)
$n_{\rm CRE,r}$	$3^{+1.5}_{-1}$	$3^{+1.5}_{-1}$	12^{+6}_{-8} (4.5)	12^{+6}_{-8} (4.5)
$n_{\rm d,r}$	3^{+10}_{-1}	3^{+10}_{-1}	<16 (5.1)	12+6$_{-8}$ (4.5)
β_s	$-3.0^{+0.05}_{-0.1}$	$-3.0^{+0.05}_{-0.1}$	$-3.1^{+0.1}_{-0.7}$ (<0.05)	$-3.1^{+0.1}_{-0.7}$ (<0.05)
$\beta_{\rm d}$	1.4 ± 0.1	$1.4^{+0.2}_{-0.4}$	$1.5^{+0.5}_{-0.3}$ (0.05)	$1.5^{+0.5}_{-0.3}$ (0.05)

Notes. For simulations with turbulence, *Simu II*, we give the variance among the set of simulation results for each parameter.

field decreases the discriminatory power of the method for all parameters but only for the radial scales of the relativistic electron and dust grain distributions does it prevent an useful measurement. The small degree of bias the results in simulations including the turbulent component show that this component should not strongly affect the results with the real *Planck* data in polarisation, since it remains small compared to the uncertainties.

We conclude that data we should be able simultaneously to constrain the models of synchrotron and thermal dust emissions parameters with the *Planck* data. In particular, we expect to constrain the direction of the Galactic magnetic field at large scales and the relative contributions of the regular and the istotropic turbulent component of the Galactic magnetic field without using external datasets. With respect to the current analysis, the

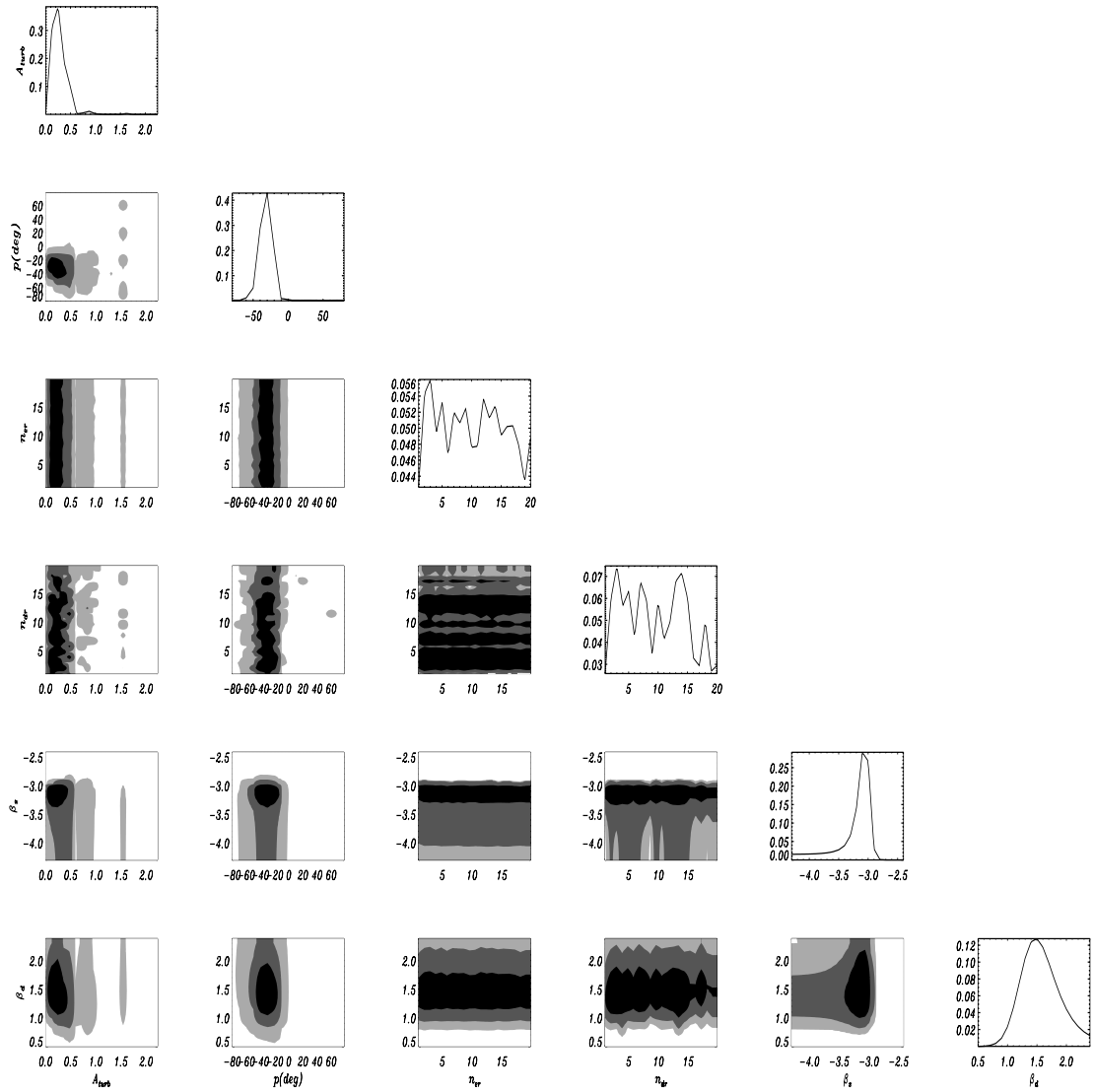

Fig. 3. Marginalised likelihood in 1 and 2D for the parameters $A_{\rm turb}$ and p, $n_{\rm CRE,r}$, $n_{\rm d,r}$, β_s and $\beta_{\rm d}$ for the (*Simu II Var*) case present the 1 (68.8%), 2 (95.4%) and 3σ (98%) confidence level contours. The values of the parameters included in the simulated data are set to $A_{\rm turb} = 0$, $p = -30°$, $n_{\rm CRE,r} = n_{\rm d,r} = 3$ kpc, $\beta_s = -3.0$, $\beta_{\rm d} = 1.4$, respectively.

Table 5. Best-fit parameters for the Galactic polarised emission models for $\beta_{\rm d} = 2.0$ in the simulated data.

Simulation	Simu I		Simu II	
$\beta_{\rm simu}$	Cst	Var	Cst	Var
$A_{\rm turb}$	<0.1	<0.1	$0.35^{+0.2}_{-0.1}$ (0.06)	$0.35^{+0.2}_{-0.1}$(0.06)
p(deg)	-30^{+4}_{-6}	-30^{+4}_{-6}	-30^{+12}_{-14} (7.5)	-30^{+12}_{-14} (7.5)
$n_{\rm CRE,r}$	$3^{+1.5}_{-1}$	$3^{+1.5}_{-1}$	12^{+6}_{-8} (4.1)	12^{+6}_{-8} (4.1)
$n_{\rm d,r}$	3^{+10}_{-1}	3^{+10}_{-1}	<16 (2)	12^{+6}_{-8} (2)
β_s	$-3.0^{+0.05}_{-0.1}$	$-3.0^{+0.05}_{-0.1}$	$-3.1^{+0.1}_{-0.7}$ (0.05)	$-3.1^{+0.1}_{-0.7}$ (0.05)
$\beta_{\rm d}$	2.0 ± 0.1	$2.0^{+0.2}_{-0.4}$	$2.2^{+0.5}_{-0.3}$ (0.05)	$2.3^{+0.5}_{-0.3}$ (0.05)

Notes. For simulations with turbulence, *Simu II*, we give the variance among the set of simulation results for each parameter.

constraints on the dust grain density parameters could be improved if the total intensity data at the *Planck* HFI channels from 100 to 857 GHz were included. More generally, a more precise reconstruction of the matter distribution in the Galaxy would require on the one hand an improved modelling of the ISM and on the other hand extra data sets, such as rotation measurements of pulsars given in Han et al. (2004) and Sun et al. (2008). These rotation measurement data along with the total intensity should also help to constrain the ordered turbulent Galactic magnetic field (see Jaffe et al. 2010), which was not considered here.

References

Alves, M., Davies, R., Dickinson, C., et al. 2010, MNRAS
Battistelli, E., Rebolo, R., Rubiñõ-Martin, J., et al. 2006, ApJ, 645, 141
Bennett, C., Halpern, M., Hinshaw, G., et al. 2003, ApJS, 148, 1
Benoît, A., Ade, P., Amblard, A., et al. 2004, A&A, 424, 571

Bersanelli, M., Mandolesi, N., Butler, R., et al. 2010, A&A, 520, A4
Boulanger, F., Abergel, A., Bernard, J.-P., et al. 1996, A&A, 312, 181
Brouw, N., & Spoelstra, T. 1976, A&AS, 26, 129
Cho, J., & Lazarian, A. 2010, ApJ, 720, 1181
Cho, J., Lazarian, A., & Vishniac, E.-T. 2002, ApJ, 285, 109
Cordes, J., & Lazio, T. 2002 [arXiv:astro-ph/0207156]
Davis, B., & Greenstein, J. 1951, ApJ, 114, 206
Désert, F.-X., Boulanger, F., & Puget, J.-L. 1990, A&A, 237, 215
Dickinson, C., Davies, R., & Davis, R. 2003, MNRAS, 341, 369
Drimmel, R., & Spergel, D. 2001, ApJ, 556, 181
Duncan, A., Reich, P., Reich, W., & Furst, E. 1999, A&A, 350, 447
Dupac, X., & Tauber, J. 2005, A&A, 430, 363
Efstathiou, G., Gratton, S., & Paci, F. 2009, MNRAS, 397, 1355
Eisenhauer, F., Schodel, R., Genzel, R., et al. 2003, ApJ, 597, L121
Fauvet, L., Macías-Pérez, J. F., Aumont, J., et al. 2010, A&A, 526, A145
Finkbeiner, D. P., Davis, M., & Schlegel, D., J. 1999, ApJ, 524, 867
Gold, B., Odegard, N., Weiland, J. L., et al. 2009, ApJS, 180, 265
Górski, K., Hivon, E., Banday, A., et al. 2005, ApJ, 622, 759
Han, J. L., Ferrière, K., & Manchester, R. N. 2004, A&A, 610, 820
Han, J. L., Manchester, R., Lyne, A., Qiao, G. J., & van Straten, W. 2006, A&A, 642, 868
Haslam, C., Salter, C., Stoffel, H., & Wilson, W. E. 1982, A&AS, 47, 1
Higdon, J.-C. 1984, ApJ, 285, 109
Hildebrand, R. H., Dotson, J., Dowell, C., Schleuning, D. A., & Vaillancourt, J. E. 1999, ApJ, 516, 834
Hinshaw, G., Nolta, M., Bennett, C., et al. 2007, ApJS, 170, 288
Hinshaw, G., Weiland, J., Hill, R., et al. 2009, ApJS, 180, 225
Jaffe, T., Leahy, J., Banday, A., et al. 2010, MNRAS, 401, 1013
Jansson, R., Farrar, G., Waelkens, A., & Ensslin, T. 2009, JCAP, 7, 21
Kogut, A., Dunkley, J., Bennett, C., et al. 2007, ApJ, 665, 355
Komatsu, E., Dunkley, J., Nolta, M., et al. 2009, ApJS, 180, 330
Lamarre, J.-M., Puget, J., Bouchet, F., et al. 2010, A&A, 520, A9
Lawson, K., Mayer, C., Osborne, J., & Parkinson, M. 1987, MNRAS, 225, 307
Lewis, A., Challinor, A., & Lasenby, A. 2000, ApJ, 538, 473
Lyne, A., & Smith, F. 1989, MNRAS, 237, 533
Macías-Pérez, J., Lagache, G., Maffei, B., et al. 2007, A&A, 467, 1313
Mandolesi, N., Bersanelli, M., Butler, R., et al. 2010, A&A, 520, A3
Mennella, A., Bersanelli, M., Butler, R., et al. 2011, A&A, 536, A3
Neugebauer, G., Habing, H. J., van Duinen, R., et al. 1984, ApJ, 278, 1
Nolta, M. 2009, ApJS, 180, 296
Page, L., Hinshaw, G., Komatsu, E., et al. 2007, ApJS, 170, 335
Planck Collaboration 2005, Planck: the Scientific Program, Vol. 1 (ESA-SCI)
Planck Collaboration 2011a, A&A, 536, A1
Planck Collaboration 2011b, A&A, 536, A19
Planck Collaboration 2011c, A&A, 536, A21
Planck Collaboration 2011d, A&A, 536, A24
Planck Collaboration 2011e, A&A, 536, A25
Planck HFI Core Team 2011, A&A, 536, A4
Ponthieu, N., Macías-Pérez, J., & Tristram, M. 2005, A&A, 444, 327
Reich, P., & Reich, W. 1988, A&AS, 74, 7
Reich, P., Reich, W., & Testori, J. 2004, The magnetised interstellar medium, ed. B. U. R. Wielebinski (Copernicus GmbH)
Reid, M., & Brunthaler, A. 2005, in Future Directions in High Resolution Astronomy: The 10th Anniversary of the VLBA, ed. J. R. M. Reid (San Fransisco: ASP), ASP Conf. Ser., 340, 253
Rybicki, G., & Lightman, A. 1979, Radiative Process in Astrophysics (New York: Wiley-Interscience)
Sun, X., Reich, W., Waelkens, A., & Ensslin, T. 2008, A&A, 477, 573
Tauber, J. A., Mandolesi, N., Puget, J. L., & Bouchet, F. 2010, A&A, 520, A1
Uyaniker, B., Furst, E., Reich, W., Reich, P., & Wielebinski, R. 1999, A&AS, 138, 31
Vaillancourt, J. E. 2002, ApJS, 142, 335
Wolleben, M., Landecker, T., Reich, W., & Wielebinski, R. 2006, A&A, 448, 411